Long-Distance Superexchange between Semiconductor Quantum-Dot Electron Spins

Haifeng Qiao,[1] Yadav P. Kandel,[1] Saeed Fallahi,[2,3] Geoffrey C. Gardner,[3,4]
Michael J. Manfra,[2,3,4,5] Xuedong Hu,[6] and John M. Nichol[1,*]

[1]*Department of Physics and Astronomy, University of Rochester, Rochester, New York 14627, USA*
[2]*Department of Physics and Astronomy, Purdue University, West Lafayette, Indiana 47907, USA*
[3]*Birck Nanotechnology Center, Purdue University, West Lafayette, Indiana 47907, USA*
[4]*School of Materials Engineering, Purdue University, West Lafayette, Indiana 47907, USA*
[5]*School of Electrical and Computer Engineering, Purdue University, West Lafayette, Indiana 47907, USA*
[6]*Department of Physics, University at Buffalo, Buffalo, New York 14260, USA*

Because of their long coherence times and potential for scalability, semiconductor quantum-dot spin qubits hold great promise for quantum information processing. However, maintaining high connectivity between quantum-dot spin qubits, which favor linear arrays with nearest neighbor coupling, presents a challenge for large-scale quantum computing. In this work, we present evidence for long-distance spin-chain-mediated superexchange coupling between electron spin qubits in semiconductor quantum dots. We weakly couple two electron spins to the ends of a two-site spin chain. Depending on the spin state of the chain, we observe oscillations between the distant end spins. We resolve the dynamics of both the end spins and the chain itself, and our measurements agree with simulations. Superexchange is a promising technique to create long-distance coupling between quantum-dot spin qubits.

Heisenberg exchange coupling is an essential feature of electron spins in semiconductor quantum dots [1–16]. It results from the interplay of the Pauli exclusion principle, the electrostatic confinement potential, and the Coulomb interaction between electrons. Its electrostatic nature makes exchange-based gates extremely fast and controllable. However, exchange coupling requires wave function overlap between interacting electrons and thus only directly couples nearest neighbor electrons. With long-distance coupling and high connectivity between spin qubits essential for quantum computing, efforts to overcome this obstacle in semiconductor nanostructures remain the focus of intense research.

Superexchange is an effective exchange coupling between distant electrons, which is mediated by intermediate spins. Theoretical work has suggested myriad ways to enable superexchange and related forms of state transfer between electron spin qubits [17–23]. So far, experimental work has focused on superexchange mediated by a single intermediate entity, such as a multielectron [24], single-electron [25], or empty [26] quantum dot. A prototypical system predicted to exhibit superexchange, which has so far not been experimentally investigated, consists of a strongly coupled spin chain [18,19,22]. If two qubits are weakly coupled to a strongly interacting spin chain, an effective exchange coupling between the two qubits emerges. This interaction, known as "superexchange," couples distant spins by virtually exciting the intermediate spins. Superexchange can mediate direct

long-distance state transfer [17,20,23] and remote entanglement [18,19] without using anything other than the qubits themselves.

In this work, we present evidence for superexchange coupling between distant electrons using a linear array of four electron spins [Fig. 1(a)]. When we properly configure the spin state of the chain, which consists of the two interior spins, and when we weakly couple the end spins to the chain, we observe oscillations between the end spins. Using adiabatic quantum state transfer (AQT) [27], we directly correlate the states of the end spins, and we also resolve the dynamics of the chain itself [Fig. 1(b)]. AQT is analogous to stimulated adiabatic Raman passage, which transfers population in a three-level quantum system. Here, we use AQT to manipulate the spin states in dots 1–3, to facilitate initialization and readout [Fig. 1(b)] [28]. Our work verifies key theoretical predictions of spin-chain-mediated superexchange in spin systems, and our results are directly extensible to superexchange over longer distances in semiconductor quantum-dot spin chains.

We describe the linear four-spin system with the following Hamiltonian:

$$H = \frac{j}{4}\boldsymbol{\sigma}_1 \cdot \boldsymbol{\sigma}_2 + \frac{J}{4}\boldsymbol{\sigma}_2 \cdot \boldsymbol{\sigma}_3 + \frac{j}{4}\boldsymbol{\sigma}_3 \cdot \boldsymbol{\sigma}_4. \quad (1)$$

Here, $\boldsymbol{\sigma}_i = \{\sigma_i^x, \sigma_i^y, \sigma_i^z\}$ represents spin i. J is a strong exchange coupling between the middle two spins, which form the chain. $j \ll J$ is a weak exchange coupling
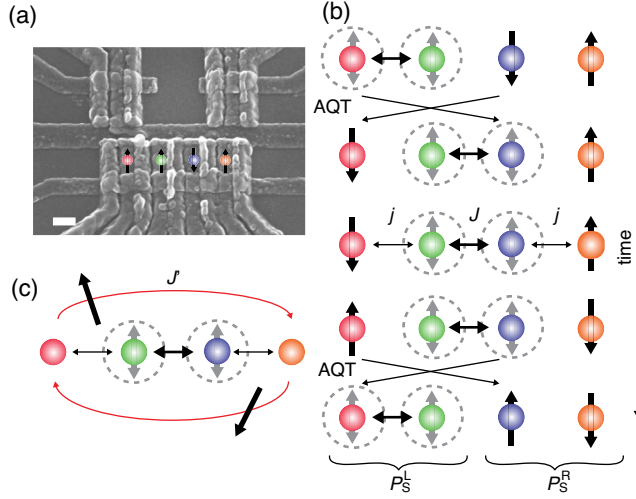
FIG. 1. (a) Scanning electron micrograph of the quadruple quantum-dot device. The positions of the electron spins are overlaid. The scale bar is 200 nm. The two quantum dots above the main array are sensor quantum dots. (b) Experimental procedure. After initializing the left pair as a singlet, we transfer that state to the middle two spins (the "chain") by AQT. We induce weak coupling j between the end spins and the chain. This configuration is predicted to induce superexchange. Another AQT step transfers the state of the chain back to the left pair and the end spins to the right pair for measurement. (c) Strong coupling among the members of a spin chain, together with weak coupling between the end spins and the chain, gives rise to a superexchange coupling J' between the end spins.

between either of the end spins and one of the chain spins. As discussed in the Supplemental Material [29], when $j \ll J$, superexchange between the end spins can occur when the chain is configured as a singlet, via virtual excitation to the polarized triplet configurations, and at an oscillation frequency of

$$J' = \frac{j^2}{2J}\left(1 + \frac{3j}{2J}\right), \tag{2}$$

up to third order in j [29]. If the chain is prepared in any of the triplet states, the chain itself evolves in time at a frequency scale of j. In this case, the evolution of the chain cannot be easily disentangled from the end-spin dynamics, so that superexchange between the end spins cannot occur with a reasonable fidelity.

In practice, we use a GaAs/AlGaAs quadruple quantum-dot device with overlapping gates to realize a coupled four-spin system [36,37] [Fig 1(a)]. The device has one electron in each dot in the symmetric configuration [38,39]. We model the exchange couplings in our system using the Heitler-London framework [40], enabling us to independently and simultaneously control the exchange couplings in this system.

We use adiabatic quantum state transfer for initialization and readout of the four-spin system [Fig. 1(b)] [27]. To this end, we configure the array into pairs of singlet-triplet

qubits ("left" and "right"). Typically, we initialize the left pair as a singlet, and the right pair as a product state with zero total spin z component S_z. Thus, the four-spin system has $S_z = 0$. The orientation of the spins in the product state depends on the sign of the local hyperfine gradient and fluctuates randomly between runs [2,3]. We transfer the singlet to the chain via AQT [Fig. 1(b)]. After this step, the initial product state of the right pair is passed to electrons 1 and 4, making their spin states random individually but always opposite to each other. As discussed further below, we can also rotate the singlet in the chain to a triplet state $|T_0\rangle$ to explore how the end-spin dynamics depend on the state of the chain.

The system evolves under the influence of a strong exchange coupling J between the electrons in dots 2 and 3 and a weaker exchange coupling j between dots 1–2 and 3–4. We measure the system by reversing the AQT sequence discussed above [Fig. 1(b)]. Provided that the state of the chain remains substantially a singlet, this process maps the state of the chain back onto the left pair, and the product state back onto the right pair. (We discuss the limiting factors of the state transfer process below.) We measure the left pair in the singlet-triplet basis and the right pair via adiabatic charge transfer (which maps the product states $|\uparrow\downarrow\rangle$ and $|\downarrow\uparrow\rangle$ to the singlet and triplet states, respectively, depending on the sign of the hyperfine gradient) followed by a Pauli spin blockade measurement [2,3]. Figures 1(b) and 1(c) summarize the experimental procedure. A high singlet probability from either pair indicates that the pair of spins returns to its initial configuration. A low singlet probability means that the pair of spins occupies an orthogonal spin state.

As discussed above, for an even-numbered spin chain, superexchange occurs when the chain (here, spins 2 and 3) is initialized in the ground state of the Heisenberg Hamiltonian (here, a singlet) [22,23]. To begin, we set $j = 45$ MHz, and we sweep J from 90 to 160 MHz. After a variable evolution time, we measure both the chain and the end spins [Figs. 2(a) and 2(b)]. We observe prominent oscillations between the end spins [Fig. 2(b)]. Figure 2(a) shows that at small values of J, the state of the chain also oscillates in time, but at large values of J, the amplitude of these oscillations diminishes. The excitation of the chain is also visible in Fig. 2(b) for low values of J, where the rapid chain oscillations appear as a distortion of the slower end-spin oscillations. The excitation of the chain is also faintly visible in the inset of Fig. 2(b). This behavior is in agreement with our expectations, because when $j \ll J$ does not hold, the chain is excited and evolves away from its ground state. Figure 2(b) also shows that the oscillation frequency between end spins decreases with J, in agreement with our expectations. Our expectations concerning the dynamics of this four-spin system are supported by detailed numerical simulations, as discussed in the Supplemental Material [29].
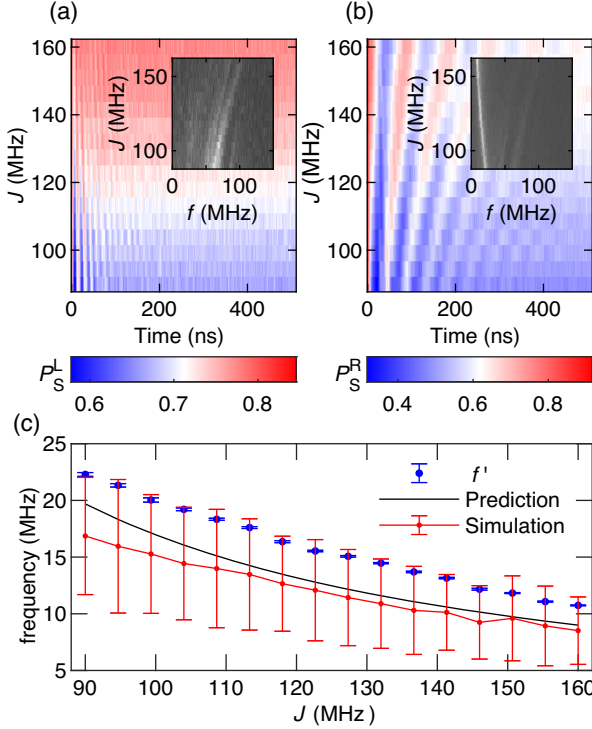
FIG. 2. Four-spin dynamics versus J with the chain initialized as a singlet. (a) Left-pair singlet return probability P_S^L versus J and evolution time showing the dynamics of the chain. Inset: absolute value of the fast Fourier transform of the data. (b) Right-pair singlet return probability P_S^R versus J and interaction time demonstrating spin-state oscillations between end spins. Inset: absolute value of the fast Fourier transform of the data. f indicates frequency. (c) Extracted end-spin oscillation frequency f' versus J. f' is the fitted frequency of the end-spin oscillations in (b) and corresponds to the peak frequencies in the inset of (b). Theoretical predictions generated from Eq. (2) and from numerical simulations are also shown. The error bars associated with the data are the standard errors of the fitted frequencies corresponding to each horizontal line in (b). The error bars associated with the simulation are the standard deviations of Monte Carlo simulations of the superexchange frequency [29]. These error bars illustrate the expected size of systematic errors associated with calibration of the exchange couplings.

The data of Figs. 2(a) and 2(b) are in good agreement with numerical simulations [29]. We extract the frequency of the observed end-spin oscillations f' from Fig. 2(b), and plot it in Fig. 2(c). In the case where the end spins oscillate under superexchange, we expect that $f' = J'$. Qualitatively, our measurements follow the $\sim 1/J$ trend of Eq. (2). We also generate quantitative predictions for the superexchange frequency using Eq. (2) and numerical simulations, as described in the Supplemental Material [29]. We find reasonably good agreement between these predictions for J' and the extracted frequencies f'.

Our measured values of f' are generally larger than the theoretical or numerically simulated values. A likely reason for this difference is an imperfect calibration of the exchange couplings, which we expect to be accurate within about 10 MHz [40]. The calibration method we use involves modeling the electronic wave function shifts during gate voltage pulses based on experimental measurements of individual exchange couplings [40]. This method is prone to underestimating the gate voltages required to induce multiple simultaneous exchange couplings [40] that are close in magnitude. The relative discrepancy between the predictions and our measurements also appears to decrease when j and J are more widely separated, which is consistent with the hypothesis that our calibration errors cause the discrepancy. A close inspection of Fig. 2(a) reveals that the actual values of J are likely lower than the target values of 90–160 MHz. The peak in the inset of Fig. 2(a), for example, occurs at a lower frequency than the target value of J. This systematic error would likely generate larger end-spin oscillation frequencies than predicted based on the target values of J alone. An additional source of error in our exchange-coupling calibration results from the fluctuating hyperfine gradient, which we did not stabilize in these experiments.

In Fig. 3 we fix J at 130 MHz, and sweep j from 10 to 50 MHz. In this case, we observe that the end-spin oscillation frequency increases with j, in agreement with our expectation from Eq. (2). Moreover, the oscillations associated with the chain become more pronounced when j increases, and the system moves farther out of the expected superexchange regime. Figure 3(c) displays the observed frequency of end-spin oscillations f' versus j along with predictions based on Eq. (2) and numerical simulations [29], showing reasonably good agreement.

As discussed above, spin-chain-mediated superexchange depends on the spin state of the chain. In general, for even-numbered chains, the ground state of the chain is non-degenerate and is thus the ideal configuration for super-exchange [23]. For a two-spin chain, the ground state (a singlet) is the only spin state that can mediate exchange. To test this prediction, we initialize the chain as a triplet $|T_0\rangle$. To achieve this, we first initialize the chain as a singlet. Then, we adiabatically ramp J to 0. This maps the singlet to either $|\uparrow\downarrow\rangle$ or $|\downarrow\uparrow\rangle$, depending on the sign of the hyperfine gradient between dots 2 and 3. Then, we perform a SWAP gate [36] between spins 2 and 3. This causes a transition between $|\uparrow\downarrow\rangle$ and $|\downarrow\uparrow\rangle$, or vice versa. After the SWAP gate, we adiabatically ramp J back to its target value, and the chain spin state is a $|T_0\rangle$. We then evolve the system with nonzero j and J. To read out the array, we reverse the ramp and SWAP sequence and then transfer the states as discussed above.

We set $j = 45$ MHz as before, and sweep J. We observe oscillations associated with both the chain and the end spins, as shown in Fig. 4. In contrast to the data of Figs. 2 and 3, however, these oscillations are short-lived, generally decaying before 200 ns. Compared with the oscillations of Fig. 3, their amplitude is smaller, and the oscillation
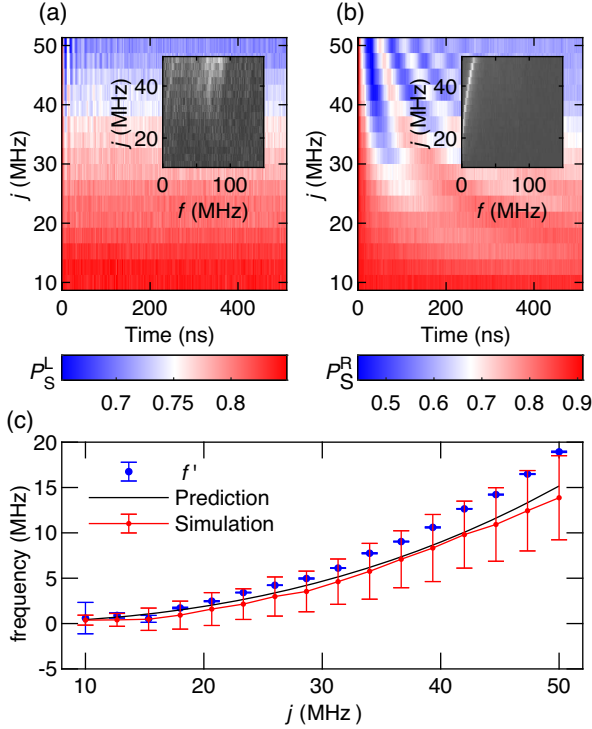
FIG. 3. Four-spin dynamics versus j with the chain initialized as a singlet. (a) Left-pair singlet return probability P_S^L versus j and evolution time showing the dynamics of the chain. Inset: absolute value of the fast Fourier transform of the data. (b) Right-pair singlet return probability P_S^R versus j and interaction time demonstrating end-spin oscillations. Inset: absolute value of the fast Fourier transform of the data. f indicates frequency. (c) Extracted end-spin oscillation frequency f' versus j. f' is the fitted frequency of the end-spin oscillations in (b) and corresponds to the peak frequencies in the inset of (b). Theoretical predictions generated from Eq. (2) and from numerical simulations are also shown. The error bars are computed as discussed above.

FIG. 4. Four-spin dynamics versus J with the spin-chain initialized as a triplet. (a) Left-pair singlet return probability P_S^L versus J and evolution time showing the dynamics of the chain. Inset: absolute value of the fast Fourier transform of the data. (b) Right-pair singlet return probability P_S^R versus J showing the dynamics of the end spins. Inset: absolute value of the fast Fourier transform of the data.

frequency does not depend substantially on J. We attribute these oscillations to rapid mixing between the different triplet configurations of the chain, not superexchange between the end spins. As before, these data are in good agreement with numerical simulations, as discussed in the Supplemental Material [29].

Having confirmed the predicted dependence of the end-spin oscillations on J, j, and the spin state of the chain, we consider the data of Figs. 2 and 3 as strong evidence for superexchange. These data mark the first evidence of superexchange between semiconductor quantum-dot electrons separated by more than one intermediary.

Some comments are in order. First, we note that the accessible ranges of J and j in our device only marginally satisfy the requirement for $j \ll J$. For this device, the large pulse amplitude required to induce exchange between dots 1 and 2, especially when other exchange couplings in the device are nonzero, limits the maximum value of J. Exchange between dots 2–3 and 3–4 does not require such
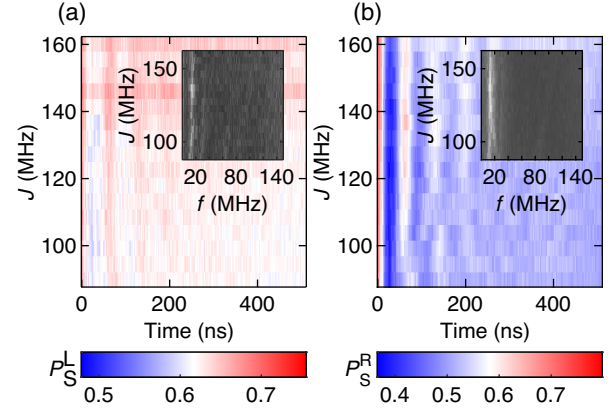
large voltage pulses. We therefore suspect the presence of a defect, likely introduced during fabrication, near dot 1 or 2. We expect that exchange couplings in future devices, especially in those with narrow barrier gates, can easily satisfy $j \ll J$. We also note that even though we only marginally satisfy $j \ll J$, our numerically simulated frequencies agree reasonably well with the theoretical values (Figs. 2 and 3).

The small uncertainty associated with j and J we have hypothesized does not pose a significant problem for future experiments harnessing superexchange. The superexchange frequency J' can easily be adjusted *in situ* without detailed knowledge of j or J, as long as $j \ll J$. Superexchange gate times can also be adjusted for given values of j and J to maximize the fidelity of superexchange operations.

Second, when the chain occupies the singlet state, our measurement procedure involving adiabatic state transfer faithfully transmits the singlet to the left pair and the z component of the end spin to the right pair [27]. However, when the chain does not have the singlet configuration, it can evolve between the triplet states during superexchange, as we have discussed above. When the chain occupies a triplet state, the adiabatic state transfer may not transfer the states with as high a fidelity, as discussed in Ref. [28]. Nonetheless, based on our simulations discussed in the Supplemental Material [29], we expect that for the range of parameters studied here, our measurement of the evolution frequencies of the chain and the end spins are not affected by the measurement process.

Third, we expect that this work is directly applicable to silicon spin qubits, where substantially reduced hyperfine fields lead to extended electron spin coherence. Symmetric exchange coupling [38], as well as Pauli-spin blockade initialization and measurement [41,42], both of which are

beneficial for superexchange, are now routine in Si/SiGe qubits. Encouragingly, recent work in Si/SiO$_2$ spin qubits has uncovered evidence of superexchange [25]. Extended arrays of Si quantum dots [43] have also been developed, and such systems are ideal for superexchange. Theoretical exploration of superexchange in Si qubits will also be necessary, however, to discover how valley splittings and couplings, as well as magnetic gradients and charge noise [42], affect superexchange.

Fourth, these results directly point the way toward superexchange in longer spin systems. Previous theoretical work has shown that Heisenberg antiferromagnets can easily be prepared by annealing a dimerized chain of singlets into the Heisenberg ground state [44,45]. We have recently shown that AQT is a straightforward and effective way to prepare singlets in arbitrary locations in quantum-dot spin chains. Our simulations also show that the superexchange frequency drops slowly with chain length [29].

In conclusion, we have presented evidence for long-distance superexchange between electron spins in semiconductor quantum dots. In the future, a complete verification of this effect will involve two-qubit quantum process tomography. In view of recent advances in silicon spin-based quantum computing, the prospects for achieving this goal are encouraging. Because high connectivity and remote entanglement between electron spins are challenges of paramount significance for spin-based quantum computing, and given the vast array of theoretical possibilities exploiting superexchange, this work presents a promising development and a significant step forward for quantum-dot spin qubits.

————

[*]john.nichol@rochester.edu

[1] D. Loss and D. P. DiVincenzo, Phys. Rev. A **57**, 120 (1998).
[2] J. R. Petta, A. C. Johnson, J. M. Taylor, E. Laird, A. Yacoby, M. D. Lukin, C. M. Marcus, M. P. Hanson, and A. C. Gossard, Science **309**, 2180 (2005).
[3] S. Foletti, H. Bluhm, D. Mahalu, V. Umansky, and A. Yacoby, Nat. Phys. **5**, 903 (2009).
[4] E. A. Laird, J. M. Taylor, D. P. DiVincenzo, C. M. Marcus, M. P. Hanson, and A. C. Gossard, Phys. Rev. B **82**, 075403 (2010).
[5] J. Medford, J. Beil, J. M. Taylor, S. D. Bartlett, A. C. Doherty, E. I. Rashba, D. P. DiVincenzo, H. Lu, A. C. Gossard, and C. M. Marcus, Nat. Nanotechnol. **8**, 654 (2013).
[6] Z. Shi, C. B. Simmons, J. R. Prance, J. K. Gamble, T. S. Koh, Y.-P. Shim, X. Hu, D. E. Savage, M. G. Lagally, M. A. Eriksson, M. Friesen, and S. N. Coppersmith, Phys. Rev. Lett. **108**, 140503 (2012).
[7] D. Kim, Z. Shi, C. B. Simmons, D. R. Ward, J. R. Prance, T. S. Koh, J. K. Gamble, D. E. Savage, M. G. Lagally, M. Friesen, S. N. Coppersmith, and M. A. Eriksson, Nature (London) **511**, 70 (2014).
[8] K. Eng, T. D. Ladd, A. Smith, M. G. Borselli, A. A. Kiselev, B. H. Fong, K. S. Holabird, T. M. Hazard, B. Huang, P. W. Deelman, I. Milosavljevic, A. E. Schmitz, R. S. Ross, M. F. Gyure, and A. T. Hunter, Sci. Adv. **1**, e1500214 (2015).
[9] Y.-P. Shim and C. Tahan, Phys. Rev. B **93**, 121410(R) (2016).
[10] A. Sala and J. Danon, Phys. Rev. B **95**, 241303(R) (2017).
[11] M. Russ, J. R. Petta, and G. Burkard, Phys. Rev. Lett. **121**, 177701 (2018).
[12] A. Sala, J. H. Qvist, and J. Danon, Phys. Rev. Research **2**, 012062 (2020).
[13] D. P. DiVincenzo, D. Bacon, J. Kempe, G. Burkard, and K. B. Whaley, Nature (London) **408**, 339 (2000).
[14] K. C. Nowack, M. Shafiei, M. Laforest, G. E. D. K. Prawiroatmodjo, L. R. Schreiber, C. Reichl, W. Wegscheider, and L. M. K. Vandersypen, Science **333**, 1269 (2011).
[15] D. M. Zajac, A. J. Sigillito, M. Russ, F. Borjans, J. M. Taylor, G. Burkard, and J. R. Petta, Science **359**, 439 (2018).
[16] M. J. Gullans and J. R. Petta, Phys. Rev. B **100**, 085419 (2019).
[17] S. Bose, Phys. Rev. Lett. **91**, 207901 (2003).
[18] A. Wójcik, T. Łuczak, P. Kurzyński, A. Grudka, T. Gdala, and M. Bednarska, Phys. Rev. A **72**, 034303 (2005).
[19] L. Campos Venuti, C. Degli Esposti Boschi, and M. Roncaglia, Phys. Rev. Lett. **96**, 247206 (2006).
[20] S. Bose, Contemp. Phys. **48**, 13 (2007).
[21] M. Friesen, A. Biswas, X. Hu, and D. Lidar, Phys. Rev. Lett. **98**, 230503 (2007).
[22] S. Oh, M. Friesen, and X. Hu, Phys. Rev. B **82**, 140403(R) (2010).
[23] S. Oh, L.-A. Wu, Y.-P. Shim, J. Fei, M. Friesen, and X. Hu, Phys. Rev. A **84**, 022330 (2011).
[24] F. K. Malinowski, F. Martins, T. B. Smith, S. D. Bartlett, A. C. Doherty, P. D. Nissen, S. Fallahi, G. C. Gardner, M. J. Manfra, C. M. Marcus, and F. Kuemmeth, Nat. Commun. **10**, 1196 (2019).
[25] K. W. Chan, H. Sahasrabudhe, W. Huang, Y. Wang, H. C. Yang, M. Veldhorst, J. C. C. Hwang, F. A. Mohiyaddin, F. E. Hudson, K. M. Itoh, A. Saraiva, A. Morello, A. Laucht, R. Rahman, and A. S. Dzurak, arXiv:2004.07666.
[26] T. A. Baart, T. Fujita, C. Reichl, W. Wegscheider, and L. M. K. Vandersypen, Nat. Nanotechnol. **12**, 26 (2017).
[27] D. Bacon and S. T. Flammia, Phys. Rev. Lett. **103**, 120504 (2009).
[28] Y. P. Kandel, H. Qiao, S. Fallahi, G. C. Gardner, M. J. Manfra, and J. M. Nichol, arXiv:2007.03869.

[29] See Supplemental Material at http://link.aps.org/supplemental/10.1103/PhysRevLett.126.017701, which includes Refs. [30–35], for further information on experimental procedures, calculations, and simulations.

[30] T. A. Baart, M. Shafiei, T. Fujita, C. Reichl, W. Wegscheider, and L. M. K. Vandersypen, Nat. Nanotechnol. **11**, 330 (2016).

[31] A. R. Mills, D. M. Zajac, M. J. Gullans, F. J. Schupp, T. M. Hazard, and J. R. Petta, Nat. Commun. **10**, 1063 (2019).

[32] S. J. Angus, A. J. Ferguson, A. S. Dzurak, and R. G. Clark, Nano Lett. **7**, 2051 (2007).

[33] D. M. Zajac, T. M. Hazard, X. Mi, K. Wang, and J. R. Petta, Appl. Phys. Lett. **106**, 223507 (2015).

[34] D. J. Reilly, C. M. Marcus, M. P. Hanson, and A. C. Gossard, Appl. Phys. Lett. **91**, 162101 (2007).

[35] C. Barthel, D. J. Reilly, C. M. Marcus, M. P. Hanson, and A. C. Gossard, Phys. Rev. Lett. **103**, 160503 (2009).

[36] Y. P. Kandel, H. Qiao, S. Fallahi, G. C. Gardner, M. J. Manfra, and J. M. Nichol, Nature (London) **573**, 553 (2019).

[37] H. Qiao, Y. P. Kandel, S. K. Manikandan, A. N. Jordan, S. Fallahi, G. C. Gardner, M. J. Manfra, and J. M. Nichol, Nat. Commun. **11**, 3022 (2020).

[38] M. D. Reed, B. M. Maune, R. W. Andrews, M. G. Borselli, K. Eng, M. P. Jura, A. A. Kiselev, T. D. Ladd, S. T. Merkel, I. Milosavljevic, E. J. Pritchett, M. T. Rakher, R. S. Ross, A. E. Schmitz, A. Smith, J. A. Wright, M. F. Gyure, and A. T. Hunter, Phys. Rev. Lett. **116**, 110402 (2016).

[39] F. Martins, F. K. Malinowski, P. D. Nissen, E. Barnes, S. Fallahi, G. C. Gardner, M. J. Manfra, C. M. Marcus, and F. Kuemmeth, Phys. Rev. Lett. **116**, 116801 (2016).

[40] H. Qiao, Y. P. Kandel, K. Deng, S. Fallahi, G. C. Gardner, M. J. Manfra, E. Barnes, and J. M. Nichol, Phys. Rev. X **10**, 031006 (2020).

[41] A. M. Jones, E. J. Pritchett, E. H. Chen, T. E. Keating, R. W. Andrews, J. Z. Blumoff, L. A. De Lorenzo, K. Eng, S. D. Ha, A. A. Kiselev, S. M. Meenehan, S. T. Merkel, J. A. Wright, L. F. Edge, R. S. Ross, M. T. Rakher, M. G. Borselli, and A. Hunter, Phys. Rev. Applied **12**, 014026 (2019).

[42] E. J. Connors, J. J. Nelson, and J. M. Nichol, Phys. Rev. Applied **13**, 024019 (2020).

[43] D. M. Zajac, T. M. Hazard, X. Mi, E. Nielsen, and J. R. Petta, Phys. Rev. Applied **6**, 054013 (2016).

[44] M. Lubasch, V. Murg, U. Schneider, J. I. Cirac, and M.-C. Bañuls, Phys. Rev. Lett. **107**, 165301 (2011).

[45] U. Farooq, A. Bayat, S. Mancini, and S. Bose, Phys. Rev. B **91**, 134303 (2015).